iScience

CellPress
OPEN ACCESS

Article

Resolving the missing link between single platelet force and clot contractile force

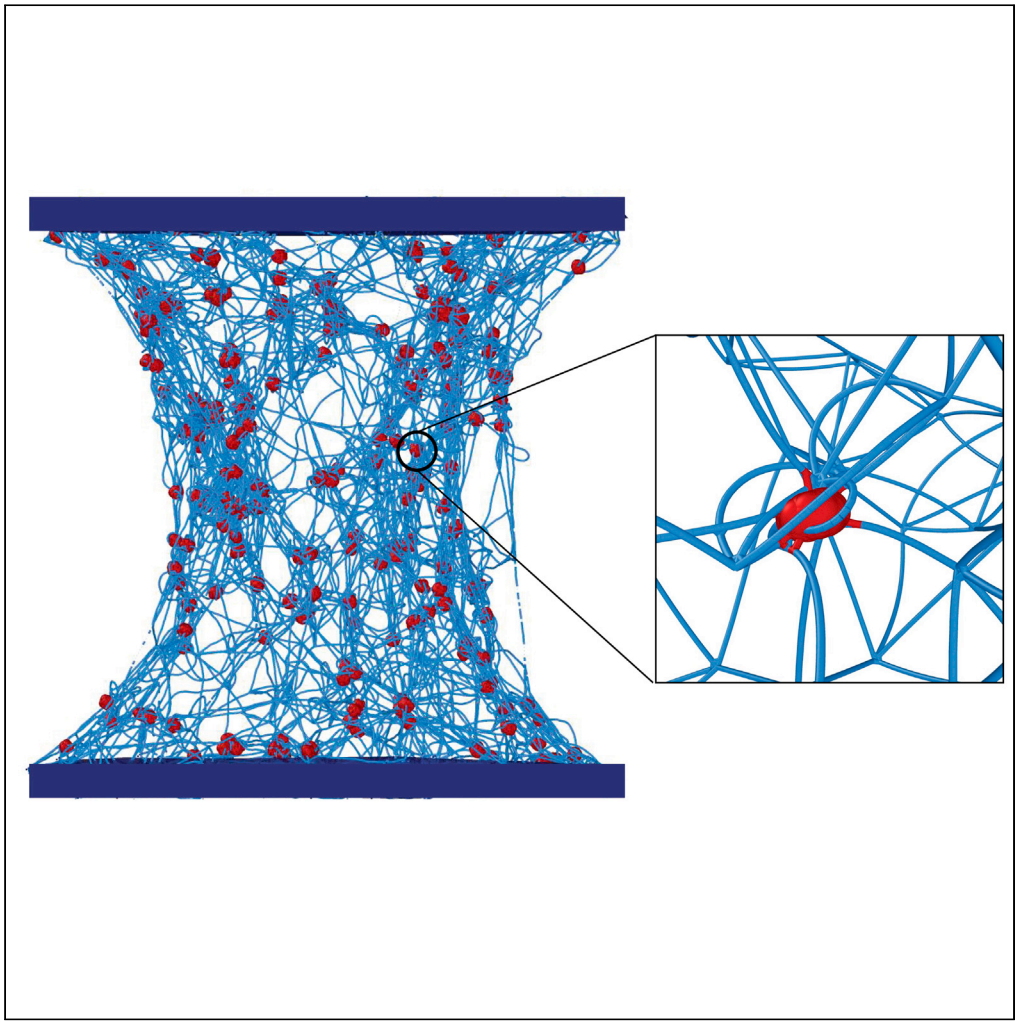

Yueyi Sun, Oluwamayokun Oshinowo, David R. Myers, Wilbur A. Lam, Alexander Alexeev

alexander.alexeev@me.gatech.edu

Highlights

Single platelet forces are measured using contraction cytometer

Computational model predicts clot contraction force

Clot force is defined by number of platelets in clot cross section

Platelets modulate force depending on mechanical microenvironment

Sun et al., iScience 25, 103690
January 21, 2022
https://doi.org/10.1016/j.isci.2021.103690

iScience

CellPress
OPEN ACCESS

Article

Resolving the missing link between single platelet force and clot contractile force

Yueyi Sun,[1] Oluwamayokun Oshinowo,[2,3,4,5,6] David R. Myers,[2,3,5,6] Wilbur A. Lam,[2,3,4,5,6] and Alexander Alexeev[1,7,*]

SUMMARY

Blood clot contraction plays an important role in wound healing and hemostasis. Although clot contraction is known to be driven by platelets, how single platelet forces relate to the forces generated by macroscopic clots remains largely unknown. Using our microfabricated high-throughput platelet contraction cytometer, we find that single platelets have an average force of 34 nN (n = 10 healthy individuals). However, multiple bulk clot experiments predict a mean single platelet force lower than 0.5 nN. To resolve this discrepancy, we use a mesoscale computational model to probe the mechanism by which individual platelets induce forces in macroscopic clots. Our experimentally informed model shows that the number of platelets in the clot cross-section defines the net clot force. We provide a relationship between single platelet force and the clot force that is useful for better understanding of blood disorders associated with bleeding and thrombosis, and facilitates the development of platelet-based and platelet-mimetic biomaterials.

INTRODUCTION

Platelets play a critical role in blood clotting and wound healing. At vascular injury sites, a cascade of signaling events leads to the formation of a soft platelet-fibrin clot which then retracts to restore normal blood flow (Cines et al., 2013). The clot retraction is driven by platelets that actively apply contraction forces to pull in the surrounding nascent fibrin fibers. The contraction force is generated by the retraction of filopodia (Kim et al., 2017), leading to a gradual decrease of the clot size and an increase of the clot mechanical stiffness (Lam et al., 2011; Jen and Mcintire, 1982; Myers et al., 2017). Blood clot mechanical properties, such as the bulk modulus and the generated contractile forces, are correlated with the ability of platelets to contract the fibrin network (Myers et al., 2017). Despite the fact that platelets are the drivers of clot contraction and the resulting clot mechanics manifests itself in blood bleeding and clotting disorders (Myers et al., 2017; Krishnaswami et al., 2002; Williams et al., 2019; Carr, 2003), stroke (Tomasiak-Lozowska et al., 2016), coronary artery disease (Greilich et al., 1994), asthma (Tomasiak-Lozowska et al., 2017; Misztal et al., 2014), and other pathologies (Le Minh et al., 2018; White et al., 2015), how platelets work together to drive the macroscale clot contraction and what relationship exists between single platelet forces and the emerging clot force are still open questions. Although single platelets have been experimentally shown to contract with forces up to 100 nN (Lam et al., 2011; Myers et al., 2017; Schwarz Henriques et al., 2012; Williams et al., 2019), the average platelet forces evaluated using bulk clot force measurements are significantly lower (Schwarz Henriques et al., 2012). Dividing the experimentally measured bulk clot force by the number of platelets yields single platelet forces lower than 1 nN (Jen and Mcintire, 1982, Carr and Zekert, 1991; Myers et al., 2017; Cohen and De Vries, 1973; Schwarz Henriques et al., 2012).

Platelet-fibrin systems find an increasing number of applications in novel biomaterials. When a normal blood flow is restored after the injury, the contracted platelet-fibrin clots act to stabilize wound fields, reattach tissue, protect the wound sites from external infections, release various growth factors and matrix remodeling enzymes, and support migration of cells for the tissue regeneration during the complex wound healing process (Drew et al., 2001; Clark et al., 1996). These diverse functions attributed to platelet-fibrin clots motivated researchers to focus on the development and clinical applications of platelet based biomaterials, such as platelet gel, platelet rich plasma (PRP), platelet fibrin glue (PFG), and platelet rich fibrin (PRF)

[1]George W. Woodruff School of Mechanical Engineering, Georgia Institute of Technology, 801 Ferst Drive, Atlanta, GA 30332-0405, USA

[2]Department of Pediatrics, Division of Pediatric Hematology/Oncology, Aflac Cancer Center and Blood Disorders Service of Children's Healthcare of Atlanta, Emory University School of Medicine, Atlanta, GA 30322, USA

[3]The Wallace H. Coulter Department of Biomedical Engineering, Georgia Institute of Technology and Emory University, Atlanta, GA 30332, USA

[4]Winship Cancer Institute of Emory University, Atlanta, GA 30322, USA

[5]Parker H. Petit Institute of Bioengineering and Bioscience, Georgia Institute of Technology, Atlanta, GA 30332, USA

[6]Institute for Electronics and Nanotechnology, Georgia Institute of Technology, Atlanta, GA 30332, USA

[7]Lead contact

*Correspondence: alexander.alexeev@me.gatech.edu

https://doi.org/10.1016/j.isci.2021.103690

A Experimental tools measuring platelet contractile forces

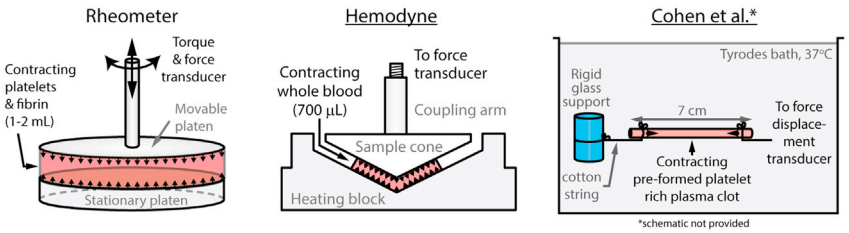

B Contractile force per platelet calculated from experimental clot force measurements

Tool	Rheometer		Hemodyne	Isometric
Author	Jen	Myers	Carr	Cohen
Platelet concentration (plt/mL)	$3x10^8$	$2.5x10^8$	$2.5x10^8$	$3.3x10^8$
Clot volume (mL)	2.0	1.5	0.7	0.9
Cross-section area (m^2)	$2.5x10^{-3}$	$2x10^{-3}$	$9x10^{-4}$	$2x10^{-5}$
Clot height (µm)	800	750	780	45837
Clot force (N)	$2.9x10^{-1}$	$1.9x10^{-1}$	$7.4x10^{-2}$	$3.5x10^{-3}$
Clot stress (N/m^2)	116	95	82	176
Contractile force per platlet (nN)	0.49	0.51	0.40	0.012

C Single platelet contractile forces measured by high-throughput cytometry

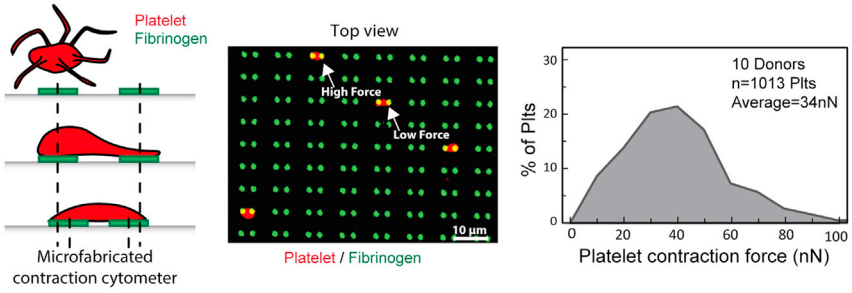

D Simulated clots contracting between walls reproduce the dynamics of clot force generation measured in experiments

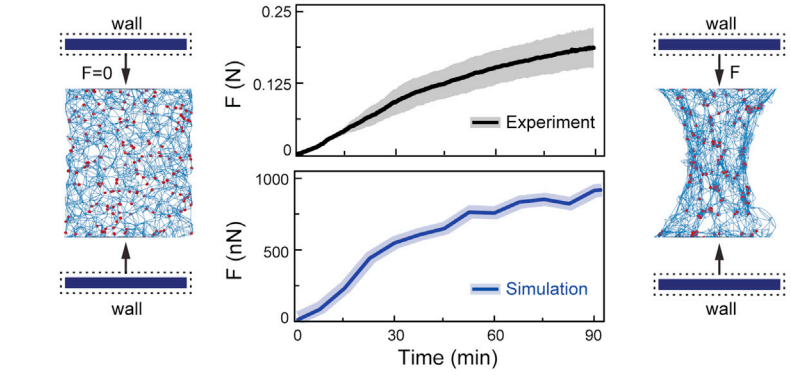

Figure 1. Mesoscale computational model connects bulk clot force with single platelet force

(A) Various experimental setups for measuring bulk clot contractile forces all of which may be used to derive contractile force per platelet. Left: rheometers suspend platelet and fibrin clots between plates and measure forces along with clot viscoelastic properties. Middle: hemodyne system measures whole blood clot contraction in a similar manner to the rheometer, although it is more streamlined for clinical use. Right: Cohen's measurement (Cohen and De Vries, 1973) are preformed after cold liquid is used to temporarily halt contraction while tying the clot to a support and transducer with cotton string.

Figure 1. *Continued*

(B) The contractile clot force per platelet calculated based on the experimental bulk clot force measurements in (A) vary from 0.012 nN to 0.51 nN.

(C) High-throughput microfabricated contraction cytometers are used here to measure single platelet forces. Left: Fibrinogen microdot pairs are covalently bound to a deformable polyacrylamide hydrogel of known mechanical properties, as a platelet adheres and pulls pairs of microdots together, the contractile force is proportional to the microdot displacement. Middle: a confocal image showing single platelets (red) contracting against fibrinogen microdot pairs (green) on the hydrogel surface. Right: histogram of measured single platelet forces from 10 healthy individuals (n = 1013 platelets).

(D) A simulated platelet-fibrin clot contracts between two parallel rigid walls, from the initial uncontracted state at t = 0 to the final contracted state at t = 90 minutes. The simulated clot applies an increasing force F on the walls, as more platelets are activated over time. The force reaches the maximum at the end of the contraction period, showing the same behavior as the experimentally measured clot force. Clot force average is represented by the solid line in each plot and standard deviation is represented by the shaded area. Simulated platelets are shown in red and fibrin fibers are in blue.

(Knighton et al., 1986; Arora and Agnihotri, 2017; Miron et al., 2017; Marx et al., 1998). Studies show that platelet derived biomaterials can be applied as effective sealing agents to reduce blood loss in surgeries (Bernasek et al., 2012), promote regeneration of tissue and bone (Nanditha et al., 2017), have significant potential for closing of nonhealing venous ulcers (O'connell et al., 2008), and can be used to induce nerve recovery across wide gaps (Kuffler et al., 2011). Although these platelet derived biomaterials vary in preparation procedure, composition and application (Arora and Agnihotri, 2017), they all rely on the clot formation and contraction processes, leading to the formation of a graft or membrane that is applied to a treated wound site. It has been reported that the mechanical strength and adhesive properties of the platelet-fibrin grafts and membranes affect cellular behaviors including cell migration and proliferation (Tse and Engler, 2011; Engler et al., 2006). Furthermore, clot mechanics affects how well the biomaterial can be molded to fit the wound site and defines the stability of the graft against unpredictable resorption (Burnouf et al., 2009), which are critical factors of successful wound healing treatments. One of the challenges in developing PRF and PGF is that the preparation procedure leads to limited volume of the material because of the clot contraction. More generally, the preparation and composition of platelet-derived biomaterials leading to the optimal therapeutic efficiency are open questions (Arora and Agnihotri, 2017). There is also a rising interest in designing semisynthetic and fully synthetic platelets that can be integrated with biomaterials to improve wound healing outcomes (Sekhon and Sen Gupta, 2017). Thus, better understanding of the physical mechanisms by which platelets contract fibrin network and how single platelet forces relate to the clot forces and material properties is needed to facilitate the future development and application of novel platelet-derived biomaterials.

Historically, two main approaches were used to evaluate the platelet contractile force. Some researchers performed force measurements of bulk clots contracting between two parallel surfaces (Figure 1A), and then calculated the contractile force per platelet by averaging the measured clot force to the number of platelets within the clot (Figure 1B) (Jen and Mcintire, 1982, Carr and Zekert, 1991; Myers et al., 2017; Cohen and De Vries, 1973). The magnitude of the contractile force per platelet varies greatly from experiment to experiment. In Cohen's experiments with clots inside siliconized glass tubes (Cohen and De Vries, 1973) this force is about 0.012 nN, whereas in the rheometer and hemodyne experiments (Jen and Mcintire, 1982; Carr and Zekert, 1991; Myers et al., 2017) it is in the range 0.4 - 0.51 nN (Figure 1B).

With the advent of new technologies, it has become possible to directly measure single platelet forces. Our system, the platelet contraction cytometer (Figure 1C), measures single platelet force with high-throughput and allows for complete control of the mechanical and biochemical microenvironments (Myers et al., 2017; Oshinowo et al., 2021). In our system, thousands of fibrinogen microdot pairs are micropatterned on a flexible polyacrylamide hydrogel surface. Platelets adhere to single microdots, spread to neighboring microdots and contract, pulling these microdots closer together. Because of the high fidelity of our microfabricated system, only a single fluorescent image is necessary to calculate the force, as contraction force is directly proportional to the microdot displacement. Here, we provide data on measurements of platelets from 10 healthy donors and show that single platelets apply forces between 1 nN and 100 nN, with an average force of about 34 nN (Figure 1C). Thus, our more comprehensive dataset broadly agrees with single platelet forces measured in other experiments (Lam et al., 2011; Schwarz Henriques et al., 2012; Williams et al., 2019).

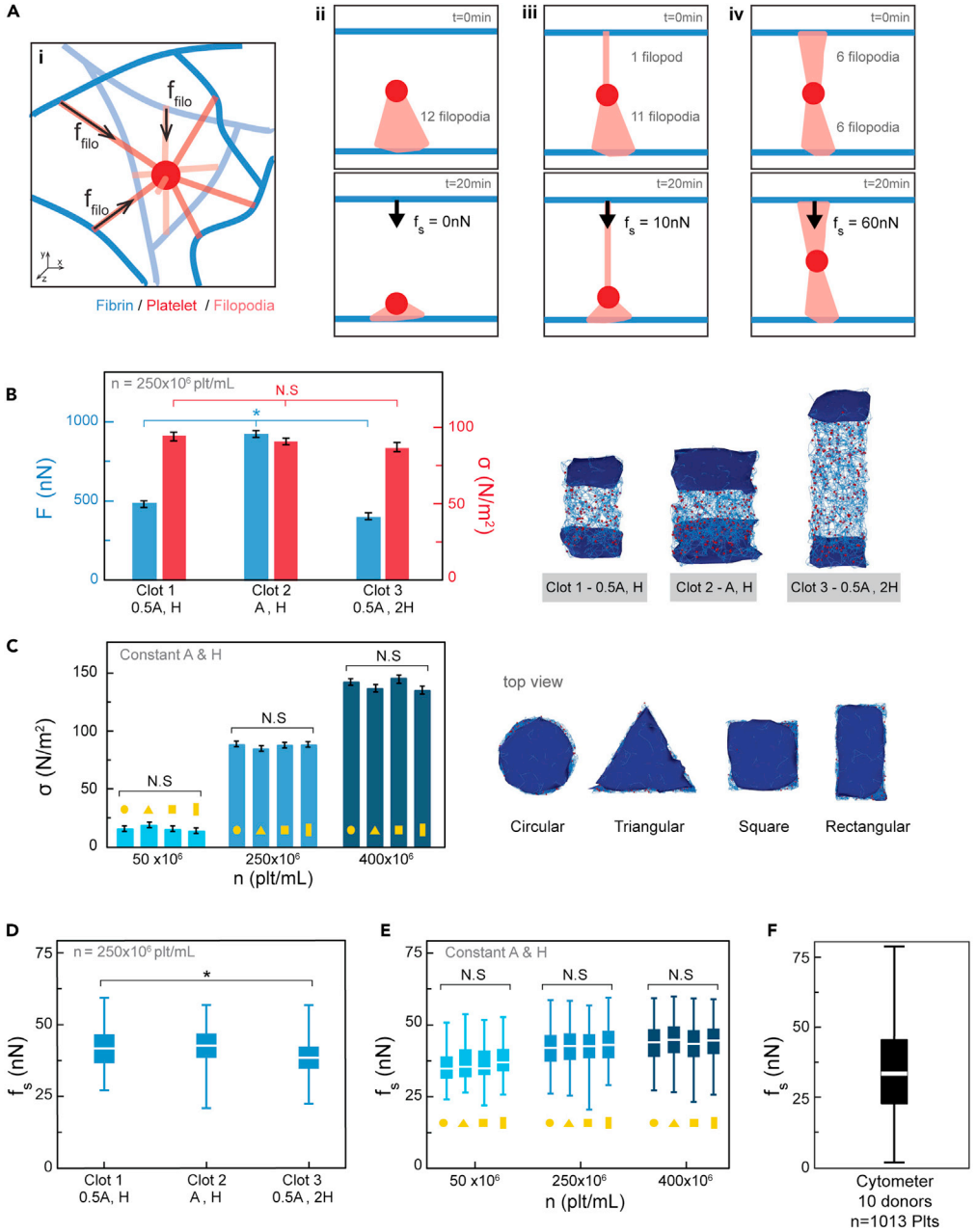

Figure 2. Clot force is proportional to clot cross-sectional area

(A) A model platelet (in red) contracts surrounding fibrin fibers (in blue) through the extension and retraction of filopodia (in pink) (i). When a platelet is suspended between two fibrin fibers, the effective force f_s applied locally by this platelet can range between 0 to 60 nN, depending on how the filopodia are distributed (ii-iv).

(B) Simulated platelet-fibrin clots 1, 2, and 3 with different combinations of A and H apply significantly different F ($p < 0.05$) but the same stress σ ($p > 0.05$) to the walls (in dark blue). The clots have constant platelet count per unit volume n = 250 × 10^6 plt/mL and volume V. Data are represented as mean +/− standard deviation. See also Video S1.

(C) At fixed n, the cross-sectional shapes of simulated platelet-fibrin clots (circular, triangular, square, rectangular) do not affect F and σ applied to the walls, $p > 0.05$ among the clots with the same n. Data are represented as mean +/− standard deviation. See also Figure S1.

(D) The platelets within simulated clots 1, 2, and 3 in (B) generate similar local single platelet forces f_s with a consistent mean value. Although statistical testing shows a significant difference between clot 1 and clot 3 ($p < 0.05$), the biological relevance of this small difference is unclear.

Figure 2. *Continued*

(E) Platelets apply consistent local single platelet forces f_s in clots with different cross-sectional geometries, $p > 0.05$ among the clots with same n. See also Figures S2 and S3. See also Video S2.

(F) Distribution of f_s in the experimental microfabricated contraction cytometer using 1013 platelets from 10 healthy donors. From (D) to (F), the boxes denote the median and quartiles, the top and bottom lines denote the maximum and minimum values, excluding the outliers. From (B) to (E), statistical analyses are performed using single factor ANOVA test, where * indicates $p < 0.05$ and N.S. indicates $p > 0.05$.

Although both the contractile force per platelet measured by bulk clot contraction and the single platelet force measurements describe platelet force during contraction, and each can be used as a clinical measure of platelet function linked to different diseases (Carr, 2003; Myers et al., 2017; Williams et al., 2019), there are 2 to 4 orders of magnitude differences between their values. The inconsistency noticed by Henriques et al. (Schwarz Henriques et al., 2012) was attributed to the complex platelet interaction causing the platelet forces to not add up linearly in clots. Although studies have been done to better understand the single platelet behavior driving the clot contraction (Myers et al., 2017; Kim et al., 2017; Lam et al., 2011; Qiu et al., 2014) and the role of platelets heterogeneity enhancing the platelet contraction efficiency (Sun et al., 2021), there is currently no experimental tool capable of monitoring the generation and transmission of forces on the single platelet level within a contracting clot. Here, we employ a mesoscale computational model to simulate the clot contraction process under physiological conditions (Sun et al., 2021). The model predicts the clot force based on the activity of individual platelets applying forces to the surrounding fibrin filaments (Figure 1D). The model allows us to closely examine the evolution of forces generated by individual platelets as they contract within a clot and evaluate the emerging clot force. Our model explicitly accounts for the properties of the fibrin mesh and platelets, including their heterogeneity, and properly captures the mechanics of clot contraction (Sun et al., 2021). Using this model we have previously demonstrated that intrinsic platelet heterogeneity leading to asynchrono-mechanical amplification plays a critical role in efficient clot contraction (Sun et al., 2021).

RESULTS AND DISCUSSION

In our simulations, we place initial platelet-fibrin clots with cross-sectional area A, height H, and volume $V = AH$, sandwiched between two rigid walls (Figure 1D). The clot is constructed from randomly oriented interconnected fibers and is populated with $N = nV$ randomly distributed platelets, where n is the platelet count per unit volume. Our model incorporates platelet biophysical heterogeneity leading to asynchronous contraction onset within platelet population and asynchronous filopodia retraction by individual platelets (Sun et al., 2021). Contraction of the clots starts at time $t = 0$ as a portion of platelets is activated, whereas other platelets remain at rest. The remaining platelets are sequentially activated during the 90 minute clot contraction period. Once a platelet is activated, it extends up to 12 filopodia in 3 successive waves that randomly grab and pull surrounding fibrin fibers, with each filopod pulls with a force that does not exceed 10 nN (Figure 2A: i). Each platelet is active for approximately 20 minutes. Because platelets are suspended in the fibrin mesh, the effective force imposed by a platelet on the surrounding fibrin fibers is $0 < f_s < 60$ nN depending on the extension and distribution of the filopodia (Figure 2A: ii-iv). This force range agrees with experimental measurements of single platelet forces (Myers et al., 2017; Lam et al., 2011; Schwarz Henriques et al., 2012). To simulate the clot contraction dynamics, platelets are sequentially activated throughout the clot contraction period to mimic platelet heterogeneity in blood clotting (Sun et al., 2021).

As the clot contracts, the clot force F applied to the wall steadily increases, consistently with the experimentally measured clot force (Figure 1D). We find that for a given platelet concentration, clots with different cross-sectional geometries, volumes ($V = AH$), and aspect ratios ($Ar = H/\sqrt{A}$) generate similar magnitudes of the normal wall stress $\sigma = F/A$ at the end of the contraction. This indicates that the clot force is proportional to the clot cross-sectional area and is independent from the clot height (Figure 2B and Video S1) and the cross-sectional shape (Figures 2C and S1).

The force F is a result of the platelet collective pulling of the fibrin mesh. Within a contracting clot, the local forces applied by active platelets vary among the platelets within the clot. As more platelets complete contraction, the average of f_s steadily increases and reaches the maximum at $t = 90$ minutes (Figure S2 and Video S2). In a fully contracted clot, f_s applied by individual platelets is distributed between 20 nN to 60 nN with an average around 40 nN (Figures 2D and 2E), matching with the experimental contraction

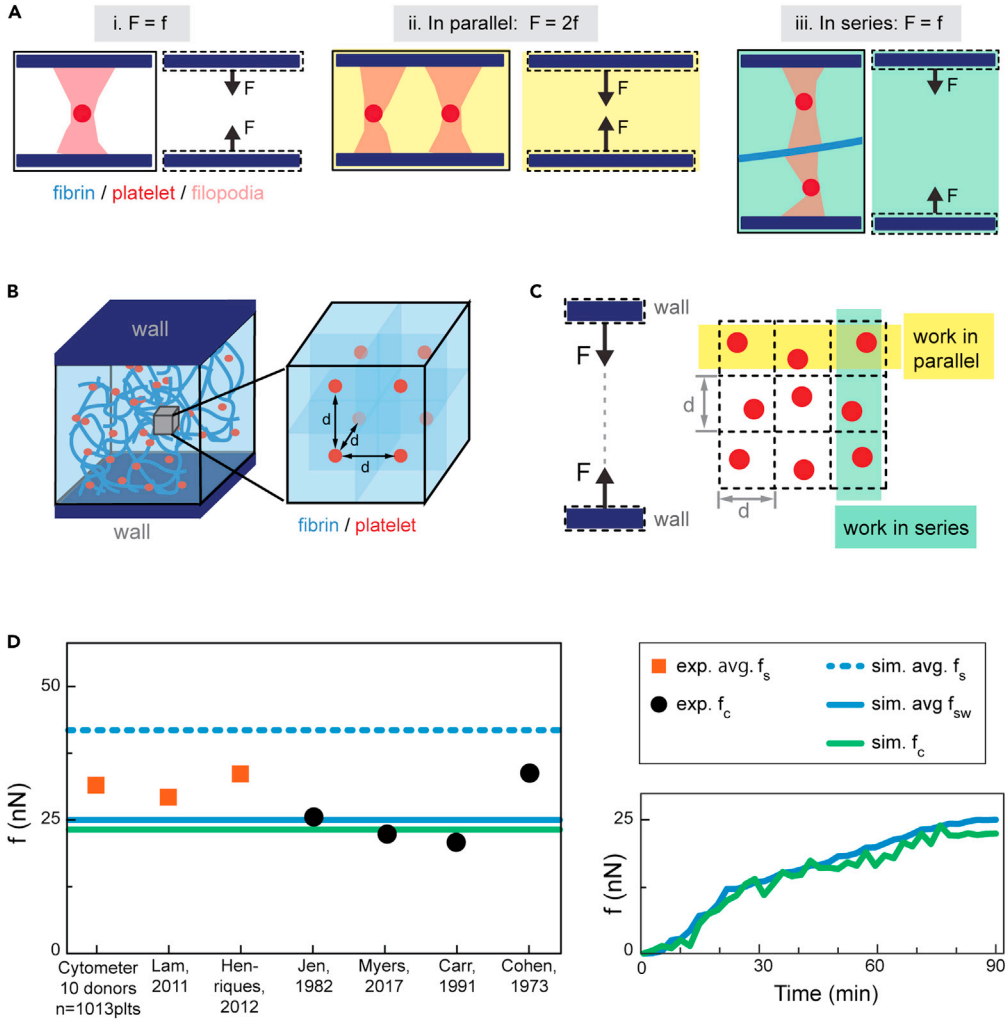

Figure 3. Clot force is proportional to number of platelets in clot cross-section

(A) Different arrangements of platelets between two parallel walls affect the overall force applied to the walls. A platelet (in red) contracting between two walls (i) applies a total force f. Two platelets arranged in parallel (ii) apply a total force 2f while two platelets arranged in series (iii) apply a total force f.

(B) When platelets are distributed uniformly inside the clot, the distance between two adjacent platelets is d.

(C) With such uniform distribution, platelets aligned in the direction of the walls contract together in parallel, and platelets aligned in the direction normal to the walls contract in series.

(D) Single platelet forces evaluated using different methods: squares denote the average of f_s measured in the experiments, circles denote f_c calculated from clot force measured in the experiments, dotted blue line denotes the average of f_s in the simulations, solid blue line denotes the average of f_{sw} in the simulations, and solid green line denotes f_c in the simulations. See also Figure S4.

cytometry measurements where 80% of platelets contracted with a force between 20 nN and 60 nN with an average force of 34 nN (Figure 2F). This force distribution is similar for clots with different cross-sectional geometries and combinations of A and H, indicating that the force applied by individual platelets is independent from these factors (Figures 2D, 2E, and S3).

To explain how F changes depending on the clot cross-sectional geometry, size, and aspect ratio, we assume simplified clot configurations where each platelet applies an equal amount of force f. When contracting platelets are arranged in parallel between two surfaces, the force $F = N_1 f$, where N_1 is the number of platelets in the layer. On the other hand, when the platelets are arranged in series, the force on the walls is limited by the single platelet force F = f (Figure 3A). Thus, the number of platelets working in parallel in a clot determines the overall clot force. To estimate the number of platelets that contract in parallel in a clot

where platelets are randomly distributed, we assume that the average distance between any adjacent platelets is $d = n^{-1/3}$ (Figure 3B). Further assuming that the platelet layer thickness is d, we estimate the number of platelets in a layer parallel to the wall is equal to $N_1 = N/(H/d) = n^{2/3}A$ (Figure 3C). Thus, the clot force is related to the single platelet force by $F = fN_1 = fn^{2/3}A$.

The above relationship can be used to evaluate the mean platelet force within a clot based on the net force exerted by the clot as $f_c = F/(n^{2/3}A)$, thereby directly connecting the single platelet force and clot force. We find that the clot forces measured in experiments (Jen and Mcintire, 1982, Carr and Zekert, 1991; Myers et al., 2017; Cohen and De Vries, 1973) yield f_c with similar values that are also close to the average of experimentally measured single platelet force f_s (Myers et al., 2017; Lam et al., 2011; Schwarz Henriques et al., 2012) (Figure 3D). When compared to our simulation results, we find close agreement with the experimental values when f_c is calculated using the simulated clot force. On the other hand, when we calculate f_s directly using the forces exerted by platelets within simulated clots, we find that in this case the average of f_s exceeds the experimental values. We related this difference to the fact that individual platelets apply force in all directions, whereas clot force is normal to the wall. Thus, f_c can somewhat underestimate the average of f_s depending on the clot boundary conditions. In our simulations, we can account for the difference between f_c and the average of f_s by only including the force component that is directed toward the wall when evaluating f_s. Indeed, the average of single platelet force normal to the wall f_{sw} shows close agreement with f_c (Figures 3D and S4).

Platelet count per unit volume n and fibrin cross-link concentration c vary as nascent clots form under different conditions that can lead to healthy and abnormal clots (Tutwiler et al., 2016). We therefore examine the contraction of clots with a wide range of platelet counts $20 \times 10^6 < n < 2000 \times 10^6$ plt/mL (Figure 4A). Note that $n < 150 \times 10^6$ plt/mL is considered as the low platelet count, whereas $n > 450 \times 10^6$ plt/mL is considered as the high platelet count. For each n we alter the fibrin cross-link concentration c which leads to varying fibrin mesh density, to probe the effect of fibrin mesh properties on clot contraction (Figure 4B).

We find that clot force is mainly determined by n, with clots containing more platelets apply greater forces at the end of the contraction period. Fibrin cross-link concentration affects clot force to a lesser extent, leading to a slightly larger F for increased c (Figure 4C). On the other hand, the single platelet force within the clot f_{sw} is practically constant at the high platelet count range and rapidly drops with n decreasing below 150×10^6 plt/mL (Figure 4D). In the high platelet count range, we find that platelets apply f_{sw} with similar magnitudes independent of c. At the same time, the clot force F is greater for higher c, indicating that an increased cross-link concentration facilitates more efficient force transmission within the clot (Figure 4D). For the entire range of platelet concentrations, f_c is in close agreement with f_{sw}, with minor deviations because of the dependence of clot force on fibrin cross-link concentration.

Remarkably, we also find that our model recapitulates platelet mechanosensing, where platelets modulate force depending on the mechanical microenvironment. In our model, contracted clots with low platelet counts have a significantly lower bulk modulus (Figure 4E). As such the platelets within the clot experience a less stiff environment leading to a decrease in the ability of the platelets to generate force (Figures 4D and 4E). We can relate this decrease in f_{sw} at low platelet counts to the inability of platelets to generate significant contractile forces in clots with a large amount of loose fibers that do not provide sufficient resistance to the filopodia retraction. In very soft clots, our model shows that the mean platelet force is approximately half the force seen in stiffer clots, and is in agreement with our contraction cytometer data. As the basic unit of our microfabricated contraction cytometer is a platelet pulling on two fibrin (ogen) dots that are covalently cross-linked to a polyacrylamide hydrogel, changing the microenvironmental stiffness experienced by single platelets can be achieved with a straightforward modification of the ratio of acrylamide to bisacrylamide in the hydrogel (Myers et al., 2017). Our calculations (Myers et al., 2017) show that 25 kPa gels recapitulate conditions associated with soft, loose fibrin networks, whereas 75 kPa gels recapitulate conditions associated with higher stiffness clots. To that end, our data shows that the average single platelet force on 25 kPa gels is approximately half of that of 75 kPa gels (Figure 4F).

To apply force on the walls, a contracting clot needs to bind the fibrin at the outer clot surfaces to the wall. Fibrin readily adsorbs on bare wall surfaces. Thus, we assume that a layer of fibrin is present on the walls to facilitate the clot-wall attachment. To investigate the effect of clot-wall attachment on the clot and platelet

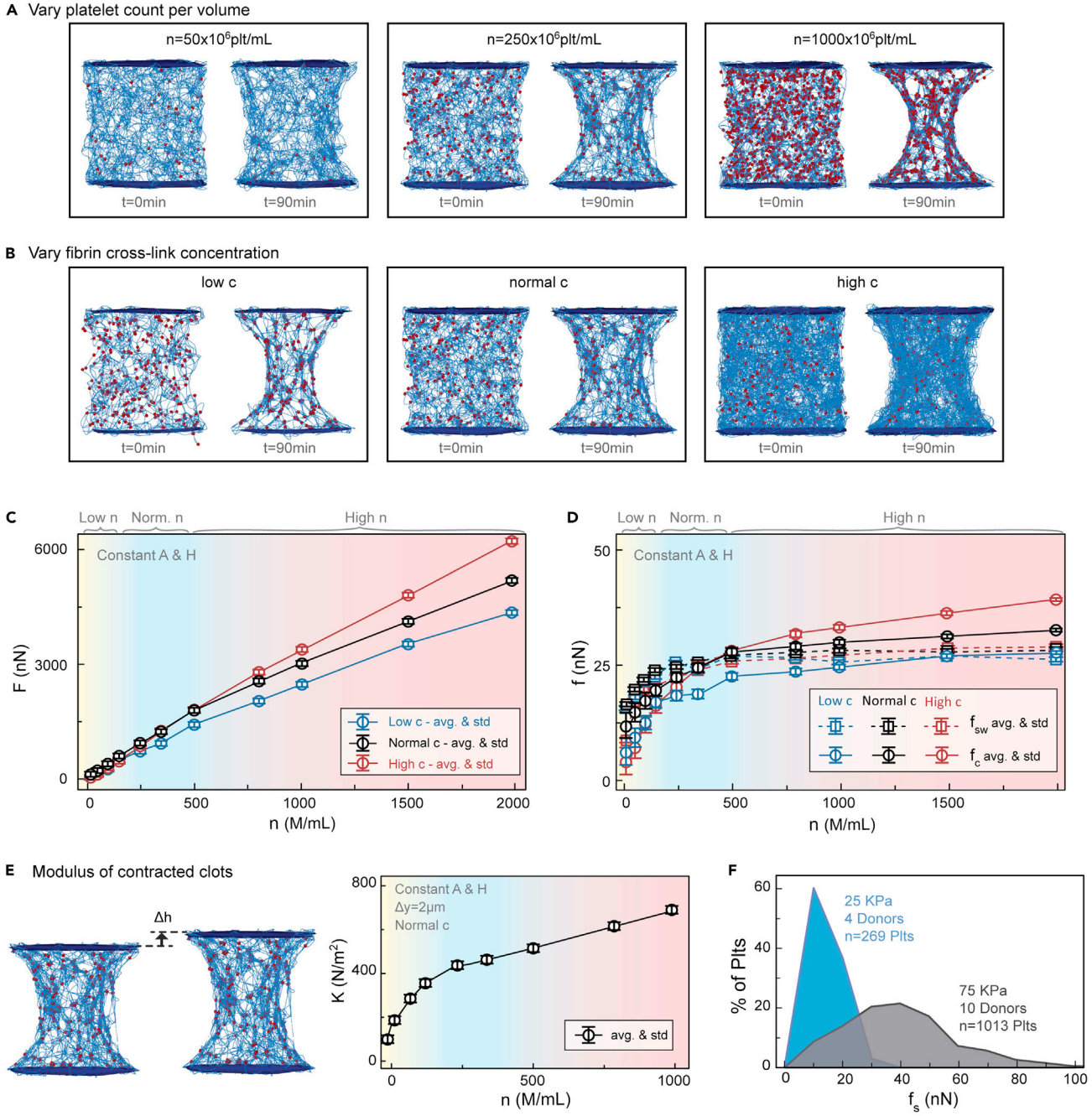

Figure 4. Clot force and single platelet force in clots with different platelet counts per unit volume and fibrin crosslink concentration

(A) The initial and final states of platelet fibrin clots with varying n contracting between two rigid walls. The clots have constant V, c, cross-section geometry.

(B) The initial and final states of platelet fibrin clots with varying c. The clots have constant V, n, cross-section geometry. In (A) and (B), platelets are shown in red, fibrin fibers are in blue, and walls are in dark blue.

(C) Clot force F applied on the walls at t = 90 min increases when the clot is populated with more platelets or contains more fibrin crosslinks.

(D) Single platelet forces at t = 90 min for clots with varying n and c.

(E) Once a clot is fully contracted in simulation, we apply additional force ΔF on the walls to increase the height of the clot by a small Δh. We calculate bulk modulus as $K = V(\Delta F/A)/\Delta V$.

(F) Experimentally measured single platelet forces with our microfabricated contraction cytometer depend on the substrate stiffness. In (C), (D), and (E), data are represented as mean +/− standard deviation.

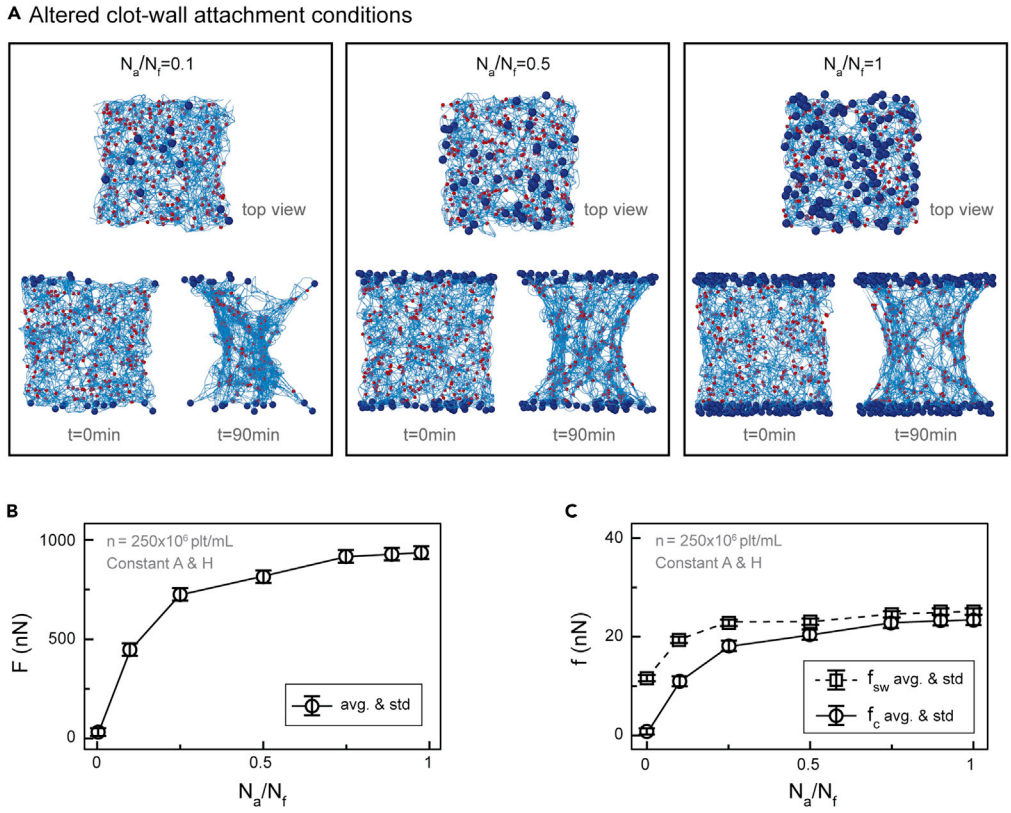

Figure 5. Clot-wall attachment affects clot and platelet forces

(A) The clots with different attachment conditions have identical V, n = 250 × 10^6 plt/mL, c, and cross-section geometry. Each dot in dark blue indicates a clot attachment point. Simulated platelets are in red, fibrin fibers are in blue, and wall beads are in dark blue. See also Figure S5.

(B) Clot force F applied on the walls at t = 90 min depends on how well the clot is attached to the walls.

(C) Single platelet force generated by platelets f_{sw} is nearly constant when the clot has sufficient attachment to the walls. When the clot is free, platelets generate lower forces. When the clot is poorly attached to the walls, it affects the clot internal homogeneity, resulting in deviation of f_c from f_{sw}. In (B) and (C), data are represented as mean +/− standard deviation.

forces, we vary the number of connection points between the clot fibrin and the wall, noted as N_a. For attaching fibrin to the wall, we use N_f potential connection points within a volume defined by a small distance δ_o away from the wall. The value of N_f is determined by the fibrin cross-link concentration c and is sufficient to have all fibers at the clot boundary attached to the wall. We examine different values of N_a in the range $0 \leq N_a/N_f \leq 1$ corresponding to varying clot-wall attachment conditions (Figures 5A and S5). Here, N_a = 0 represents a free clot that is not attached to the walls. Our results show that clot force drops significantly when the clot is poorly attached to the walls (Figure 5B). Interestingly, the force f_{sw} generated by the platelets is nearly insensitive to the attachment conditions as long as there are even a small number of connection points between the clot and the walls (Figure 5C). In the free clot situation, the net force generated by the clot is zero. Still the platelets within the clot generate a substantial force f_{sw} to deform the fibrin network and to maintain it in the contracted state. We find that f_{sw} can be successfully predicted using the clot force as $f_c = F/(n^{2/3}A)$ when $N_a/N_f \gtrsim 0.25$, and that f_c somewhat underestimates f_{sw} when the clot is poorly attached to the walls (Figure 5C). Note that for $N_a/N_f < 0.25$, the clot-wall attachment is incomplete with multiple fibers at the boundary untethered, which alters the force distribution within the contracting clot and effectively reduces its cross-sectional area (Figure 5A).

Nascent clots can form with different shapes because of the geometric constraints in the blood vessel, and the influence of the hemodynamic and external forces (Jackson, 2007). We further examine forces generated by clots contracting between tilted and non-flat walls, representing varying blood vessel geometry

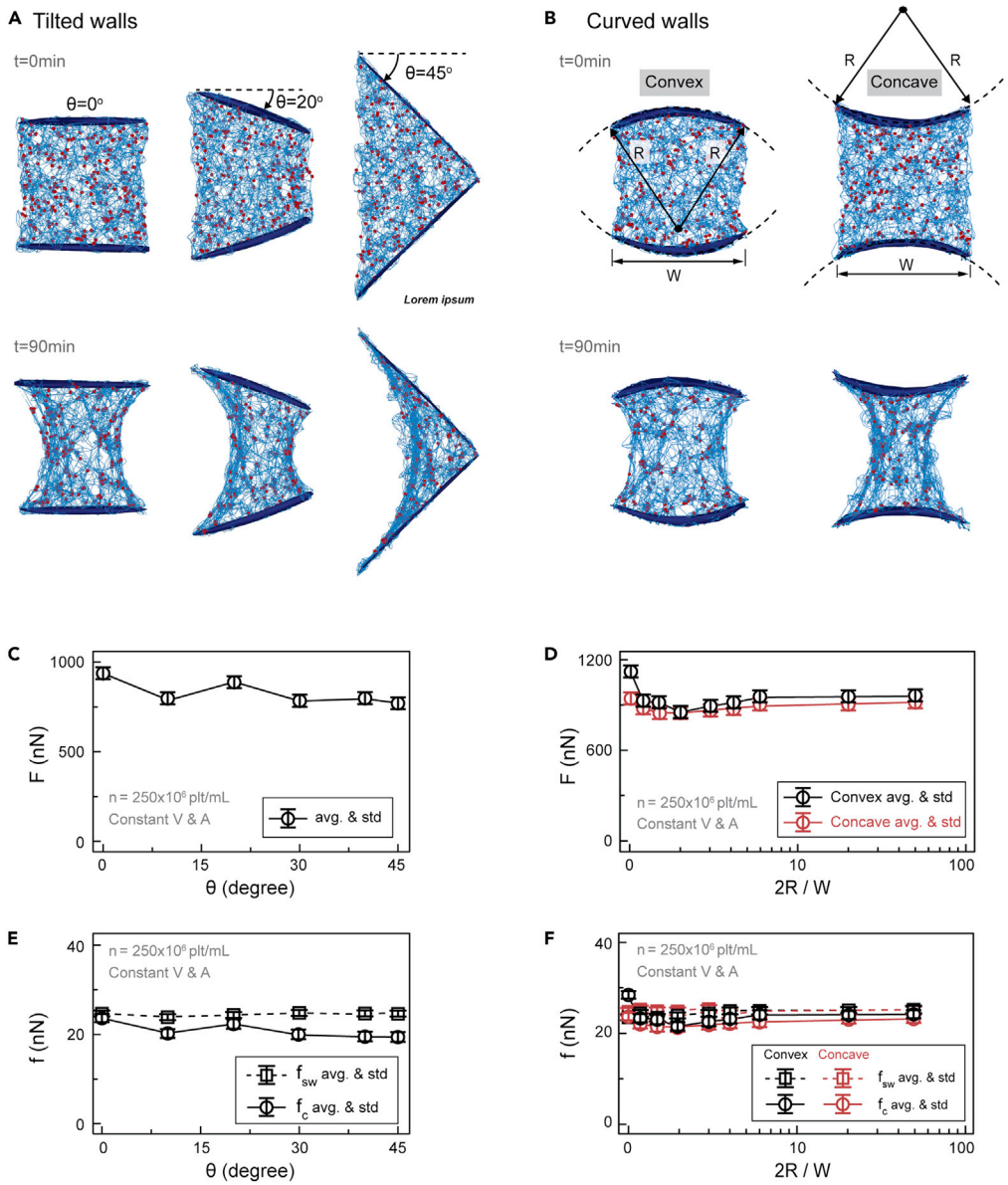

Figure 6. Effect of wall geometry on clot force and individual platelet forces

(A) The initial and final states of platelet-fibrin clots contracting between two tilted walls with varying angle θ. See also Video S3.

(B) The initial and final states of platelet-fibrin clots contracting between two curved walls (convex and concave) with varying curvature R.

The clots in (A and B) all have constant V, n, c, and cross-sectional area A of the clot normal to the direction connecting the centroids of the two walls. Platelets are shown in red and fibrin fibers are shown in blue.

(C and D) Panels show clot force F at t = 90 min for, respectively, clots contracting between tilted and curved walls.

(E and F) Panels show single platelet force in the direction of walls f_{sw} and the estimated f_c calculated based on the clot force. From (C) to (F), data are represented as mean +/− standard deviation.

constraints. In these simulations, we keep constant the clot volume V, platelet count n, and fibrin cross-link concentration c, and only vary the wall geometry. In the case of tilted walls, the walls are rotated at an angle θ from the midplane (Figure 6A), whereas for non-flat walls, the walls have a constant curvature r (Figure 6B). In all the cases, the initial cross-sectional area of the clots remains the same. We find that the resulting clot force is not affected by θ and R (Figures 6C and 6D). Thus, the simulations indicate that the wall geometry has a minor influence on the net clot force. This is consistent with our conclusion that the clot force is

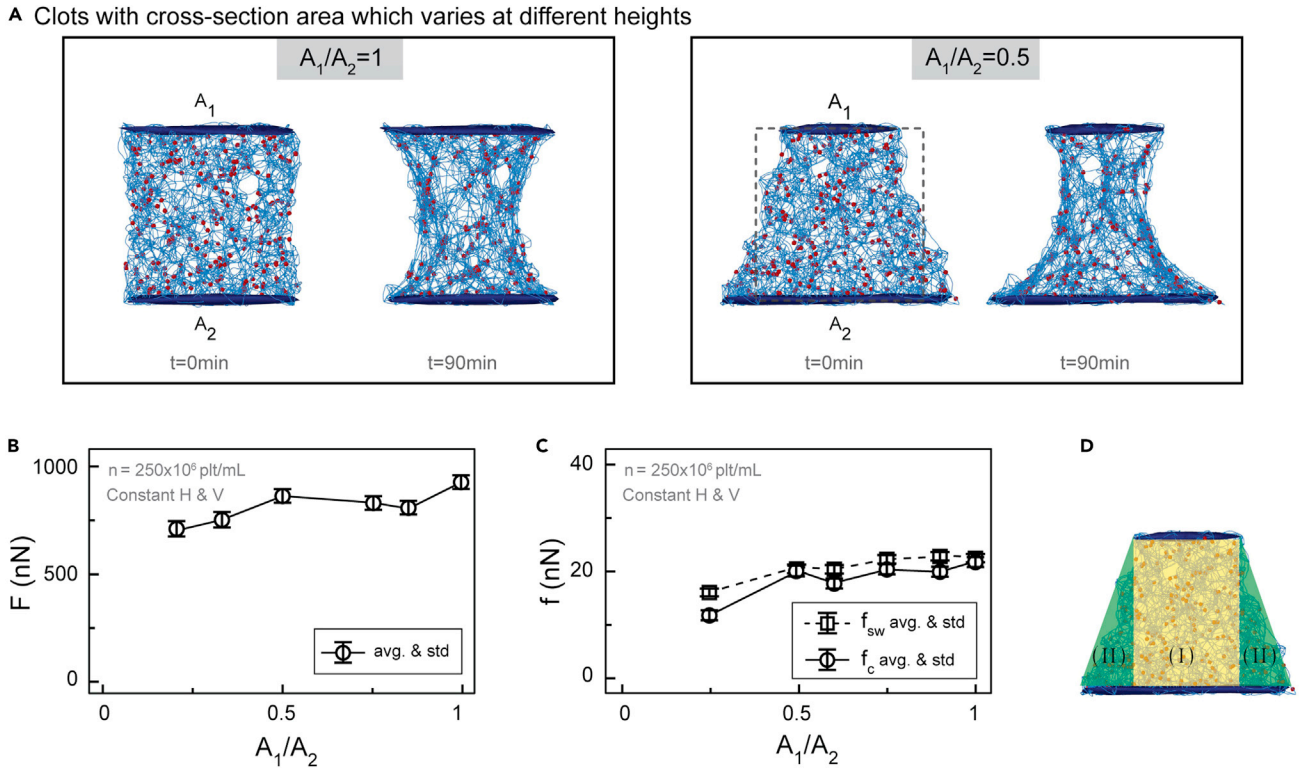

Figure 7. Clot force and single platelet force in clots with varying cross-sectional area

(A) The initial and final states of platelet fibrin clots between two parallel walls with different areas. The cross-sectional area of each clot varies linearly from one wall to the other. The clots have constant V, H, n, and c. Platelets are shown in red, fibrin fibers are in blue, and walls are in dark blue.

(B) Clot force F slightly increases as the ratio of A1/A2 increases toward unity.

(C) Average single platelet forces slightly increases with increasing A1/A2. Here, f_{sw} is obtained in the simulations by averaging forces of individual platelets and f_c is calculated based on the clot force at t = 90 min. (D). The clot geometry can be represented by two regions I and II with different attachment to the walls. In (B and C), data are represented as mean +/− standard deviation.

defined by the clot cross-sectional area and therefore the number of platelets that apply the force in parallel. We also find that the forces generated by individual platelets f_{sw} are insensitive to the wall geometry and can be successfully predicted using the clot force as $f_c = F/(n^{2/3}A)$ (Figures 6E and 6F). Note that in this case the area A is the cross-sectional area of the clot normal to the direction connecting the centroids of the opposing wall surfaces.

In Figure 7, we probe the force generated by clots with varying cross-sectional areas. Specifically, we consider clots with trapezoidal geometry where the clot cross-sectional area at the top wall A_1 is smaller than the clot cross-sectional area at the bottom wall A_2 (Figure 7A). We change the ratio A_1/A_2 by simultaneously decreasing A_1 and increasing A_2 such that the clot volume V and height H remain constant, i.e. $A_1 + A_2 = \text{const}$. We find that clot force F and single platelet force f_{sw} slightly decrease with decreasing A_1/A_2 (Figures 7B and 7C). Furthermore, the single platelet force $f_c = F/(n^{2/3}A)$ with A being the average clot cross-section area of the clot matches closely to the average f_{sw} of individual platelets within the clot (Figure 7C). These results suggest that a clot generates the maximum contracting force when its initial cross-sectional area is uniform. When $A_1 < A_2$, the clot can be represented by section I which is connected to both walls and two sections II that are only connected to the bottom wall as illustrated in Figure 7D. We relate the reduction in the clot force to the fact that sections II are unable to directly impose force on the top wall thereby reducing the net force generated by the clot. This also results in the reduction of the mean forces of the individual platelets in trapezoidal clots.

Conclusions

In an attached clot, individual platelets actively apply forces contracting nearby fibrin fibers generating the clot force and changing the clot structure and mechanical properties. We utilize an experimentally informed and

validated mesoscale computational approach to model platelet-fibrin clot contracting between two rigid walls. The single platelet dynamics is specified based on the experimental measurements of individual platelets and platelet activation patterns within the clot, whereas the fibrin mesh is constructed based on the digitization of an experimental platelet-fibrin clot (Sun et al., 2021). The model provides a unique opportunity to probe bulk clot forces, clot structural changes, and to monitor platelet forces at the level of individual filopodia during the clot contraction. We employ this model to explain how local forces of individual platelets are applied to the constraining walls through the elastic fibrin scaffold, thus establishing the connection between the single platelet force and the emerging clot force. We find that the mechanical stress within the clot is independent of the clot size and aspect ratio and is mostly defined by the platelet concentration and fibrin density. The clot force is mainly determined by the clot cross sectional area, whereas the clot height and shape have a minor effect. This result suggests that the number of platelets in the clot cross section defines the total clot force. We estimate this number and derive a relationship between the single platelet force and the net clot force. By comparing the platelet and clot forces with experimental measurements, we show that our model correctly estimates the single platelet force from the clot forces, and even recapitulates platelet mechanosensing behavior. Furthermore, the model can be used to predict the net clot force based on the platelet and clot properties. We validate that our correlation is applicable to clots with varying platelet count, fibrin cross-link concentration, wall-fibrin attachment condition, and wall geometries, thus capable of predicting the clot contraction forces for a wide range of physiologically relevant conditions. More importantly, our model provides a highly needed link between the individual platelet force measurements and bulk clot force measurements in different experiments revealing that in these previous experiments the forces on the single platelet level are roughly identical.

Our work contributes to better understanding of single platelet function, showing that platelets are able to sense and react to their surrounding microenvironment. In our model, single platelets have the ability to exert the same amount of maximum force, and the force can be applied to all directions with no preference. We notice that while platelets are contracting within fibrin scaffolds, they tend to apply a larger amount of force in the directions toward the bounding walls compared to the other directions. This is because of the fact that platelet force is related to the resistance from the local fibrin fibers. This also explains why platelets exert lower forces in the clots with low platelet counts or poor wall-fibrin attachment conditions. In these cases, multiple fibrin fibers remain unstressed and can be pulled by the platelets with lower forces. Hence, our model recapitulates the phenomenon of platelet mechanosensing, seen previously (Myers et al., 2017; Lam et al., 2011) as well as in our experiments with the highest number of single platelet measurements reported to date.

Our work establishes the correlation between the microscale cell biophysical properties and the macroscale behavior of the biological material, revealing the mechanism by which individual platelets arrange within blood clots to yield the clot force. The results of our work allow one to predict the final clot force and clot structure based on the known single platelet properties. Furthermore, our results indicate how the measured clot force can be used as an indicator of single platelet force. This could assist the development of new clinical diagnostic techniques that utilize bulk clot force measurements as indicators of different platelet deficiencies. Our findings can also be applied to contracting cells that are embedded in and contract against a scaffold beyond platelets, such as myofibroblasts, and even semisynthetic and synthetic platelets mimics. Finally, our model can facilitate the design, application, and optimization of grafts for treating wounds, composed of PRP, PRF, and platelet-inspired biomaterials. In particular our model can be useful for the engineering of platelet-based biomaterials and biomaterials with synthetic platelets with specific geometry to precisely fit the wound site to achieve the desired levels of stress and stiffness for enhanced efficacy.

Limitations of the study

Although our model captures the basic mechanism of platelet-driven clot contraction, it has limitations that can be addressed in future work. Our model does not consider platelet adhesion to the vessel wall via collagen or von Willebrand factor, although these are typical interactions occurring during the initial phase of hemostasis. Our model does not incorporate the effects of fluid flow, shear stress, and red blood cells on the clot contraction process. The size of the clot we model is relatively small limited by computational resources. Thus, the model predictions may be less accurate for large scale clots. Although our mesoscale model does not include all the factors relevant to biological clots, it is able to successfully capture the clot contraction process under physiological conditions (Sun et al., 2021). Furthermore, this approach can be further expanded to model the activity of additional cell types in biological materials.

Our model is built and validated with the platelet dynamics and bulk clot contraction process under physiological conditions of pH, salt, and temperature, allowing us to examine the mechanics of the generation of clot force, the effect of platelet concentration, fibrin network density, and clot-wall attachment on the contraction process. Note that we cannot directly examine how the clot contraction process changes because of variations in pH, salt, and temperature conditions.

STAR★METHODS

Detailed methods are provided in the online version of this paper and include the following:

- KEY RESOURCES TABLE
- RESOURCE AVAILABILITY
  - Lead contact
  - Materials availability
  - Data and code availability
- EXPERIMENTAL MODEL AND SUBJECT DETAILS
  - Human blood samples
- METHOD DETAILS
  - Experimental platelet contraction cytometry
  - Computational model of platelet-fibrin clot contracting between walls
  - Fibrin mesh
  - Platelets
  - Clot-wall attachments
  - Bulk clot force
  - Single platelet force
  - Clot contraction between flat parallel walls
  - Clot contraction between tilted and non-flat walls
- QUANTIFICATION AND STATISTICAL ANALYSIS

SUPPLEMENTAL INFORMATION

Supplemental information can be found online at https://doi.org/10.1016/j.isci.2021.103690.

ACKNOWLEDGMENTS

Financial support provided by NIH R35 (HL145000) to W.A.L.; NIH R21 (EB026591), NIH K25 (HL141636), & NIH R01 (HL155330) to D.R.M., NSF 1809566 to W.A.L. and D.R.M., NIH F31 (HL160210-01) and American Society of Hematology Minority Medical Student Award Program Fellowship to O.O. and NSF 1809227 to A.A. The work uses the Extreme Science and Engineering Discovery Environment (XSEDE) provided through Award TG-DMR180038.

AUTHOR CONTRIBUTIONS

Y.S., D.R.M., W.A.L., and A.A. planned the work. Y.S. developed the computational model and carried out the simulations. O.O. and D.R.M. carried out the experiments. Y.S., D.R.M., W.A.L., and A.A. interpreted the data and wrote the manuscript.

DECLARATION OF INTERESTS

The authors declare no competing interests.

INCLUSION AND DIVERSITY

One or more of the authors of this paper self-identifies as an underrepresented ethnic minority in science.

Received: September 7, 2021
Revised: November 4, 2021
Accepted: December 20, 2021
Published: January 21, 2022

REFERENCES

Arora, S., and Agnihotri, N. (2017). Platelet derived biomaterials for therapeutic use: review of technical aspects. Indian J. Hematol. Blood Transfus. *33*, 159–167. https://doi.org/10.1007/s12288-016-0669-8.

Bernasek, T.L., Burris, R.B., Fujii, H., Levering, M.F., Polikandriotis, J.A., and Patterson, J.J. (2012). Effect on blood loss and cost-effectiveness of pain cocktails, platelet-rich plasma, or fibrin sealant after total knee arthroplasty. J. Arthroplasty *27*, 1448–1451. https://doi.org/10.1016/j.arth.2012.02.018.

Burnouf, T., Su, C.-Y., Radosevich, M., Goubran, H., and El-Ekiaby, M. (2009). Blood-derived biomaterials: fibrin sealant, platelet gel and platelet fibrin glue. ISBT Sci. Ser. *4*, 136–142. https://doi.org/10.1111/j.1751-2824.2009.01222.x.

Carr, M.E., Jr., and Zekert, S.L. (1991). Measurement of platelet-mediated force development during plasma clot formation. Am. J. Med. Sci. *302*, 13–18. https://doi.org/10.1097/00000441-199107000-00004.

Carr, M.E. (2003). Development of platelet contractile force as a research and clinical measure of platelet function. Cell Biochem. Biophys. *38*, 55–78. https://doi.org/10.1385/CBB:38:1:55.

Cines, D.B., Lebedeva, T., Nagaswami, C., Hayes, V., Massefski, W., Litvinov, R.I., Rauova, L., Lowery, T.J., and Weisel, J.W. (2013). Clot contraction: compression of erythrocytes into tightly packed polyhedra and redistribution of platelets and fibrin. Blood *123*, 1596–1603. https://doi.org/10.1182/blood-2013-08-523860.

Clark, R.A., Tonnesen, M.G., Gailit, J., and Cheresh, D.A. (1996). Transient functional expression of alphaVbeta 3 on vascular cells during wound repair. Am. J. Pathol. *148*, 1407–1421.

Cohen, I., and De Vries, A. (1973). Platelet contractile regulation in an isometric system. Nature *246*, 36–37.

Collet, J.P., Shuman, H., Ledger, R.E., Lee, S., and Weisel, J.W. (2005). The elasticity of an individual fibrin fiber in a clot. Proc. Natl. Acad. Sci. U S A *102*, 9133. https://doi.org/10.1073/pnas.0504120102.

Drew, A.F., Liu, H., Davidson, J.M., Daugherty, C.C., and Degen, J.L. (2001). Wound-healing defects in mice lacking fibrinogen. Blood J. Am. Soc. Hematol. *97*, 3691–3698. https://doi.org/10.1182/blood.V97.12.3691.

Engler, A.J., Sen, S., Sweeney, H.L., and Discher, D.E. (2006). Matrix elasticity directs stem cell lineage specification. Cell *126*, 677–689. https://doi.org/10.1016/j.cell.2006.06.044.

Greilich, P., Carr, M.E., Zekert, S.L., and Dent, R.M. (1994). Quantitative assessment of platelet function and clot structure in patients with severe coronary artery disease. Am. J. Med. Sci. *307*, 15–20. https://doi.org/10.1097/00000441-199401000-00003.

Groot, R.D., and Warren, P.B. (1997). Dissipative particle dynamics: bridging the gap between atomistic and mesoscopic simulation. J. Chem. Phys. *107*, 4423–4435. https://doi.org/10.1063/1.474784.

Jackson, S.P. (2007). The growing complexity of platelet aggregation. Blood. J. Am. Soc. Hematol. *109*, 5087–5095. https://doi.org/10.1182/blood-2006-12-027698.

Jen, C.J., and Mcintire, L.V. (1982). The structural properties and contractile force of a clot. Cell Motil. *2*, 445–455. https://doi.org/10.1002/cm.970020504.

Kim, O.V., Litvinov, R.I., Alber, M.S., and Weisel, J.W. (2017). Quantitative structural mechanobiology of platelet-driven blood clot contraction. Nat. Commun. *8*, 1–10. https://doi.org/10.1038/s41467-017-00885-x.

Knighton, D.R., Ciresi, K.F., Fiegel, V.D., Austin, L.L., and Butler, E.L. (1986). Classification and treatment of chronic nonhealing wounds. Successful treatment with autologous platelet-derived wound healing factors (PDWHF). Ann. Surg. *204*, 322. https://doi.org/10.1097/00000658-198609000-00011.

Krishnaswami, A., Carr, M.E., Jr., Jesse, R.L., Kontos, M.C., Minisi, A.J., Ornato, J.P., Vetrovec, G.W., and Martin, E.J. (2002). Patients with coronary artery disease who present with chest pain have significantly elevated platelet contractile force and clot elastic modulus. Thromb. Haemost. *88*, 739–744.

Kuffler, D.P., Reyes, O., Sosa, I.J., and Santiago-Figueroa, J. (2011). Neurological recovery across a 12-cm-long ulnar nerve gap repaired 3.25 years post trauma: case report. Neurosurgery *69*, E1321–E1326. https://doi.org/10.1227/NEU.0b013e31822a9fd2.

Lam, W.A., Chaudhuri, O., Crow, A., Webster, K.D., Li, T.-D., Kita, A., Huang, J., and Fletcher, D.A. (2011). Mechanics and contraction dynamics of single platelets and implications for clot stiffening. Nat. Mater. *10*, 61–66. https://doi.org/10.1038/nmat2903.

Le Minh, G., Peshkova, A.D., Andrianova, I.A., Sibgatullin, T.B., Maksudova, A.N., Weisel, J.W., and Litvinov, R.I. (2018). Impaired contraction of blood clots as a novel prothrombotic mechanism in systemic lupus erythematosus. Clin. Sci. *132*, 243–254. https://doi.org/10.1042/CS20171510.

Marx, R.E., Carlson, E.R., Eichstaedt, R.M., Schimmele, S.R., Strauss, J.E., and Georgeff, K.R. (1998). Platelet-rich plasma: growth factor enhancement for bone grafts. Oral Surg. Oral Med. Oral Pathol. Oral Radiol. Endodontol. *85*, 638–646. https://doi.org/10.1016/S1079-2104(98)90029-4.

Miron, R.J., Fujioka-Kobayashi, M., Bishara, M., Zhang, Y., Hernandez, M., and Choukroun, J. (2017). Platelet-rich fibrin and soft tissue wound healing: a systematic review. Tissue Eng. B Rev. *23*, 83–99. https://doi.org/10.1089/ten.teb.2016.0233.

Misztal, T., Rusak, T., and Tomasiak, M. (2014). Peroxynitrite may affect clot retraction in human blood through the inhibition of platelet mitochondrial energy production. Thromb. Res. *133*, 402–411. https://doi.org/10.1016/j.thromres.2013.12.016.

Myers, D.R., Qiu, Y., Fay, M.E., Tennenbaum, M., Chester, D., Cuadrado, J., Sakurai, Y., Baek, J., Tran, R., Ciciliano, J.C., et al. (2017). Single-platelet nanomechanics measured by high-throughput cytometry. Nat. Mater. *16*, 230–235. https://doi.org/10.1038/nmat4772.

Nanditha, S., Chandrasekaran, B., Muthusamy, S., and Muthu, K. (2017). Apprising the diverse facets of Platelet rich fibrin in surgery through a systematic review. Int. J. Surg. *46*, 186–194. https://doi.org/10.1016/j.ijsu.2017.08.558.

O'connell, S.M., Impeduglia, T., Hessler, K., Wang, X.J., Carroll, R.J., and Dardik, H. (2008). Autologous platelet-rich fibrin matrix as cell therapy in the healing of chronic lower-extremity ulcers. Wound Repair Regen. *16*, 749–756. https://doi.org/10.1111/j.1524-475X.2008.00426.x.

Oshinowo, O., Copeland, R., Sakurai, Y., Fay, M.E., Petrich, B.G., Leong, T., Brainard, B., and Lam, W.A. (2021). Significant differences in single-platelet biophysics exist across species but attenuate during clot formation. Blood Adv. *5*, 432–437. https://doi.org/10.1182/bloodadvances.2020003755.

Qiu, Y., Brown, A.C., Myers, D.R., Sakurai, Y., Mannino, R.G., Tran, R., Ahn, B., Hardy, E.T., Kee, M.F., Kumar, S., et al. (2014). Platelet mechanosensing of substrate stiffness during clot formation mediates adhesion, spreading, and activation. Proc. Natl. Acad. Sci. U S A *111*, 14430–14435. https://doi.org/10.1073/pnas.1322917111.

Schwarz Henriques, S., Sandmann, R., Strate, A., and Köster, S. (2012). Force field evolution during human blood platelet activation. J. Cell Sci. *125*, 3914–3920. https://doi.org/10.1242/jcs.108126.

Sekhon, U.D.S., and Sen Gupta, A. (2017). Platelets and platelet-inspired biomaterials technologies in wound healing applications. ACS Biomater. Sci. Eng. *4*, 1176–1192. https://doi.org/10.1021/acsbiomaterials.7b00013.

Sirk, T.W., Slizoberg, Y.R., Brennan, J.K., Lisal, M., and Andzelm, J.W. (2012). An enhanced entangled polymer model for dissipative particle dynamics. J. Chem. Phys. *136*, 134903. https://doi.org/10.1063/1.3698476.

Sun, Y., Myers, D.R., Nikolov, S.V., Oshinowo, O., Baek, J., Bowie, S.M., Lambert, T.P., Woods, E., Sakurai, Y., Lam, W.A., et al. (2021). Platelet heterogeneity enhances blood clot volumetric contraction: an example of asynchrono-mechanical amplification. Biomaterials *274*, 120828. https://doi.org/10.1016/j.biomaterials.2021.120828.

Tomasiak-Lozowska, M.M., Misztal, T., Rusak, T., Branska-Januszewska, J., Bodzenta-Lukaszyk, A., and Tomasiak, M. (2017). Asthma is associated with reduced fibrinolytic activity, abnormal clot architecture, and decreased clot retraction rate. Allergy *72*, 314–319. https://doi.org/10.1111/all.13054.

Tomasiak-Lozowska, M.M., Rusak, T., Misztal, T., Bodzenta-Lukaszyk, A., and Tomasiak, M. (2016). Reduced clot retraction rate and altered platelet energy production in patients with asthma. J. Asthma *53*, 589–598. https://doi.org/10.3109/02770903.2015.1130151.

Tse, J.R., and Engler, A.J. (2011). Stiffness gradients mimicking in vivo tissue variation regulate mesenchymal stem cell fate. PLoS One *6*, e15978. https://doi.org/10.1371/journal.pone.0015978.

Tutwiler, V., Litvinov, R.I., Lozhkin, A.P., Peshkova, A.D., Lebedeva, T., Ataullakhanov, F.I., Spiller, K.L., Cines, D.B., and Weisel, J.W. (2016). Kinetics and mechanics of clot contraction are governed by the molecular and cellular composition of the blood. Blood. J. Am. Soc. Hematol. *127*, 149–159. https://doi.org/10.1182/blood-2015-05-647560.

White, N.J., Newton, J.C., Martin, E.J., Mohammed, B.M., Contaifer, D., Jr., Bostic, J.L., Brophy, G.M., Spiess, B.D., Pusateri, A.E., Ward, K.R., et al. (2015). Clot formationis associated with fibrinogen and platelet forces in a cohort of severely injured emergency department trauma patients. Shock *44*, 39. https://doi.org/10.1097/SHK.0000000000000342.

Williams, E.K., Oshinowo, O., Ravindran, A., Lam, W.A., and Myers, D.R. (2019). Feeling the force: measurements of platelet contraction and their diagnostic implications. Semin. Thromb. Hemost. *45*, 285–296. https://doi.org/10.1055/s-0038-1676315.

STAR★METHODS

KEY RESOURCES TABLE

REAGENT or RESOURCE	SOURCE	IDENTIFIER
Chemicals, peptides, and recombinant proteins		
Alexa Fluor 488 tagged Fibrinogen	Fisher Scientific	F13191
Thrombin	Haematologic Technologies	HCT-0020
Calcium Chloride	Sigma-Aldrich	C4901
Magnesium Chloride	Sigma-Aldrich	M0250
HEPES	Sigma-Aldrich	H3375
Sodium Bicarbonate	Sigma-Aldrich	S5761
Potassium Chloride	Sigma-Aldrich	P3911
Sodium Chloride	Sigma-Aldrich	S9888
Glucose	Sigma-Aldrich	G8270
Cell Mask Orange 554/567	Fisher Scientific	C10045
Software and algorithms		
Large-scale Atomic/Molecular Massively Parallel Simulator (LAMMPS)	https://www.lammps.org/	LAMMPS Stable Release

RESOURCE AVAILABILITY

Lead contact

Further information and request for resources should be directed to the lead contact, Alexander Alexeev (alexander.alexeev@me.gatech.edu).

Materials availability

This study did not generate new unique reagents or resources.

Data and code availability

- Experimental platelet contraction cytometry data are available upon reasonable request by contacting the lead contact.
- All codes are available upon reasonable request by contacting the lead contact.
- Any additional information required to reanalyze the data reported in this paper is available upon reasonable request by contacting the lead contact.

EXPERIMENTAL MODEL AND SUBJECT DETAILS

Human blood samples

Consent for 10 healthy adult donor platelets (Ages 18-45, 5 males and 5 females) was obtained according to GT IRB H15258. Blood was drawn into the anticoagulant acid-citrate-dextrose (ACD) solution 2. The sample was subsequently centrifuged at 150 G for 15 min without brake and the resulting platelet rich plasma (PRP) was centrifuged again with an additional 10% ACD by volume at 900 G for 5 min without brake. The supernatant, platelet poor plasma, was discarded and platelet pellet was resuspended into HEPES modified tyrodes buffer (1 g/L $NaHCO_3$, 8.06 g/L NaCl, 1 g/L glucose, 0.216 g/L KCl, and 2.38 g/L Hepes) and was gel filtered into this same buffer (Oshinowo et al., 2021).

METHOD DETAILS

Experimental platelet contraction cytometry

Polyacrylamide hydrogels with pairs of Alexa Fluor 488 tagged fibrinogen (Fisher Scientific) microdots with a radius of .8 μm and separation of 4 μm were fabricated at a stiffness of 75 kPa or 25 kPa. 2×10^9/L

thrombin-activated platelets (1 U/mL thrombin; Haematologic Technologies) were then plated in a solution containing $CaCl_2$ (3 mM) (Sigma Aldrich) and $MgCl_2$ (3 mM) (Sigma Aldrich) for 2 hrs. A platelet will land, adhere, spread to the neighboring microdot and contract the pairs of microdots causing the patterned microdots to displace. After the 2-h incubation, platelets were tagged with Cell Mask Orange 554/567 (Fisher Scientific). As platelet force is directly proportional to the microdot displacement, only a single fluorescent image is necessary to measure the force of an individual platelet. Uncontracted pairs of microdots were utilized as the reference distance in order to calculate the displacement relative to original position. Traction forces (T) of individual platelets was calculated as:

$$T = \frac{2\pi Ga(x_s - x_f)}{2 - v}$$

where G is shear modulus, a is microdot radius, v is Poisson's ratio and x_s is the starting distance and x_f is the final distance. Platelet contraction was imaged on a Zeiss LSM 780/ELYRA PS1 confocal microscope using a 20x/0.8 NA Plan Apochromat lens (Oshinowo et al., 2021).

Computational model of platelet-fibrin clot contracting between walls

We constructed a three-dimensional model of a platelet fibrin clot contracting between two rigid walls using a mesoscale computational method, in which the platelets and fibrin mesh were modeled using bead-spring approach, and the rigid walls were modeled as groups of immobile beads. Nonbonded interaction forces between beads follow the dissipative particle dynamics (Groot and Warren, 1997) including repulsive, dissipative, and random potentials that conserve the local momentum (Sun et al., 2021). The governing dynamics among beads is set by the sum of three main forces $F = \sum_{j \neq i}(F_{ij}^C + F_{ij}^D + F_{ij}^R)$ acting between a bead i and its neighboring beads j located within a cutoff radius r_c. Here the conservative repulsive force $F_{ij}^C = a_{ij} w(r_{ij}) \hat{r}_{ij}$ represents the bead excluded volume, the dissipative force $F_{ij}^D = -\gamma w(r_{ij})^2 (r_{ij} \cdot v_{ij}) \hat{r}_{ij}$ represents the effect of viscosity, and the random force $F_{ij}^R = \sigma w(r_{ij}) \xi_{ij} (\Delta t)^{-1/2} \hat{r}_{ij}$ accounts for the thermal fluctuations. The dissipative and random forces are related by $\sigma^2 = 2\gamma k_b T$ due to the fluctuation-dissipation theorem. The interaction between bonded beads is determined by the harmonic bond potential $E_{bond} = 0.5 K_{bond} (r - r_{eq})^2$ and bending angle potential $E_{bend} = K_{bend}[1 + \cos(\theta)]$, where k_{bond} is the bond stiffness, r_{eq} is the equilibrium separation length between beads, k_{bend} is the bending stiffness, and θ is the angle between two bonds sharing a common bead. We modeled platelets contracting fibrin through filopodia retraction by dynamically creating bonds between platelets and fibrin and then gradually contracting these bonds. We modeled clot-to-wall attachments by bonding the wall and fibrin beads. The fibrin filaments were prevented from crossing each other by applying repulsion forces between bonds that are closer than a minimum distance using a segmented repulsive potential (Sirk et al., 2012). To include the effect of an implicit viscous solvent, we imposed viscous and random forces evaluated from the Langevin thermostat. The forces and velocities of all beads are integrated between each time step using the velocity Verlet algorithm to track the time evolution of the platelet-fibrin clot. In our simulations, we set the cutoff distance $r_c = 1$, $\gamma = 4.5$, $K_b T = 1$, repulsion strength $a = 25$, bead mass $m = 1$ and integration time step $\Delta t = 0.01$.

Fibrin mesh

We modeled fibrin clot mesh using semi-flexible polymer chains randomly interconnected at randomly distributed cross-link points. The cross-link points concentration was determined based on the amount of fibrin fiber intersections per unit volume found in the confocal image analysis of experimental fibrin clots prepared with 2 mg/mL of purified human fibrinogen (Sun et al., 2021). Allowing each cross-link node randomly connects to up to 5 neighbors, we obtained fibrin mesh with average fibrin filament length around 10 μm. Each fibrin filament is a polymer chain containing n beads between two cross-link points, where the beads are connected by harmonic stretching and bending potentials. We set equilibrium length $r_{eq} = 1$, bond stiffness $K_{bond} = 800$ and bending stiffness $K_{bend} = 800$ of the harmonic bonds (Sun et al., 2021) such that elastic modulus of the modeled fibrin filaments matches experimental measurements (Collet et al., 2005). We set $r_{c,SRP} = 0.5$, $C = 100$ for the segmented repulsive potential to prevent fibrin chains from crossing each other. In the simulations where we examined the effect of fibrin mesh properties, we varied the cross-link concentration while keeping the number of connected neighbors and average fibrin filament length constant to generate fibrin clots with different densities.

Platelets

We modeled platelets using clusters of interconnected beads. At rest, platelets have a disk-like shape with a 2 μm diameter and do not actively interact with other clot elements. When a platelet became active, it extended up to 12 filopodia that connect to random fibrin filaments within 6 μm from the platelet center. Filopodia retraction was achieved by gradually reducing the bond length to 1 μm with a series of small steps, with bond stiffness set to K_{bond} = 12.2. The clot was equilibrated after each contraction step. The contractile force exerted by a single filopod was limited to 10 nN. Single platelets were set to complete contraction activity within 20 minutes after activation.

For each platelet concentration, we randomly distributed the required number of platelets at rest in initial fibrin mesh to create the initial clot. Among all platelets within the clot, we randomly assigned 50% of the platelets to start contraction at the initial time t = 0, and we randomly divided rest of the platelets into 9 groups that start contraction at 9 equal time intervals, such that all platelets complete contraction at t = 90 minutes. When a platelet was activated, it extended filopodia in three waves that were uniformly distributed in time over the platelet activity period such that for each platelet the filopodia were extended and fully retracted within 20 minutes (Sun et al., 2021).

Clot-wall attachments

For each initial clot, we attached the fibrin fibers located at the fibrin mesh boundaries to the respective walls. To this end, we first identified N_f cross-link beads located within a small distance δ_o away from the wall surfaces, and then connected each of these cross-link beads to a wall bead through a harmonic bond (Figure S5). We set the equilibrium length of the harmonic bond equal to the minimum distance from the cross-link bead to wall surface and set the bond stiffness K_{bond} equal to that of fibrin filaments. To examine the effect of clot-wall attachment conditions, we selected N_a out of N_f cross-link beads where $N_a \leq N_f$, and then connected N_a cross-link beads to the wall beads with harmonic bonds.

Bulk clot force

We obtained the final clot force F as the force imposed by the clot on the wall at the end of the clot contraction process. Clot stress was calculated by dividing the clot force by the initial clot cross-sectional area normal to the direction connecting the centroids of the opposing walls. In each simulation, we evaluate the clot force and the standard deviation over 200000 timesteps after the simulation converged to a steady state.

Single platelet force

We evaluated the effective force imposed by each platelet within the clot on the surrounding fibrin filaments as $f_s = 0.5\sum f_{fil}$, where f_{fil} was the contracting force of platelet filopodia. We obtained f_{sw} as a component of f_s acting in the direction of the net clot force F. The force f_s quantifies the effective strength of platelet contraction in all directions while suspended in fibrin mesh, whereas f_{sw} quantifies the effective strength of platelet contraction in the wall direction. The magnitudes of f_s and f_{sw} were averaged over all the platelets within the clots. We evaluated the forces and the standard deviations similarly to the bulk clot calculations.

Clot contraction between flat parallel walls

We examined the effects of clot cross-sectional geometry, sizes, aspect ratio, platelet count per unit volume, and fibrin cross-link concentration on clot force generation by creating different initial platelet-fibrin clots attached to two rigid walls. Specifically, we generated initial platelet-fibrin clots with square cross-section and different combinations of H and A at platelet concentration 250 × 10^6 plt/mL and fibrin crosslink concentration 2 mg/mL: clot 1 with H = 100 μm and A = 5000 μm^2, clot 2 with H = 100 μm and A = 10000 μm^2, clot 3 with H = 200 μm and A = 5000 μm^2. To examine clots with different cross-sectional shapes, we generated initial clots with circular, square, rectangular and triangular cross-sections, with H = 100 μm, A = 10000 μm^2, and fibrin cross-link concentration 2 mg/mL. The simulations were performed at platelet concentrations 50 × 10^6 plt/mL, 250 × 10^6 plt/mL, and 400 × 10^6 plt/mL. To test clots with different platelet and fibrin cross-link concentrations, we generated initial clots with H = 100 μm and A = 10000 μm^2.

Clot contraction between tilted and non-flat walls

To examine clot contraction between tilted walls, the clots were generated between walls tilted at an angle θ from the mid-plane, where at $\theta = 0$ the walls were parallel and at $\theta = 45^{\circ}$ the walls intersected. To examine clot contraction between curved walls, we introduced a wall curvature R, where smaller R referred to more curved walls. For each curvature, convex and concave walls were tested. For each case, we kept constant the clot volume, platelet count per unit volume, fibrin cross-link concentration, and cross-section area of the clot normal to the direction connecting the wall centroids to facilitate the comparison between the walls with different geometry.

QUANTIFICATION AND STATISTICAL ANALYSIS

The data are shown as mean +/− standard deviation. The data in Figures 2D and 2E are shown as the median and quartiles, where the top and bottom lines denote the maximum and minimum values, excluding the outliers. The statistical analyses were performed using single factor ANOVA (analysis of variance) test.